Bidirectional Dc-Dc Converter Analysis And Implementation

R.S.Saipraveen Kumar
Asst. Professor, Dept of EEE
Sri Venkatesa Perumal College Of Engineering & Technology,Puttur.

Abstract- *A novel bidirectional DC-DC converter is presented in this paper. The circuit configuration of the proposed converter is very simple. The proposed converter employs a coupled inductor with same winding turns in the primary and secondary sides. In step-up mode, the primary and secondary windings of the coupled inductor are operated in parallel-charge and series-discharge to achieve high step-up voltage gain. In step-down mode, the primary and secondary windings of the coupled inductor are operated in series-charge and parallel-discharge to achieve high step-down voltage gain. Thus, the proposed converter has higher step-up and step-down voltage gains than the conventional bidirectional DC-DC boost/buck converter. Under same electric specifications for the proposed converter and the conventional bidirectional boost/buck converter, the average value of the switch-current in the proposed converter is less than the conventional bidirectional boost/buck converter. The operating principle and steady-state analysis are discussed in detail. Finally, a 14/42-V prototype circuit is implemented to verify the performance for the automobile dual-battery system.*

Keywords- bidirectional DC-DC converter, coupled inductor.

INTRODUCTION

Bidirectional DC–DC converters are used to transfer the power between two DC sources in either direction. These converters are widely used in applications, such as hybrid electric vehicle energy systems , uninterrupted power supplies , fuel-cell hybrid power systems PV hybrid power systems, and battery chargers . Many bidirectional DC-DC converters have been researched. The bidirectional DC-DC flyback converters are more attractive due to simple structure and easy control . However, these converters suffer from high voltage stresses on the power devices due to the leakage-inductor energy of the transformer. In order to recycle the leakageinductor energy and to minimize the voltage stress on the power devices, some literatures present the energyregeneration techniques to clamp the voltage stress on the power devices and to recycle the leakage-inductor energy . Some literatures research the isolated bidirectional DCDC converters, which include the half-bridge types , and full-bridge types . These converters can provide high step-up and step-down voltage gain by adjusting the turns ratio of the transformer. For non-isolated applications, the non-isolated bidirectional DC-DC converters, which include the conventional boost/buck types , multi-level type , three-level type , sepic/zeta type, switched-capacitor type , and coupled-inductor type are presented. The multi-level type is a magnetic-less converter, but 12 switches are used in this converter. If higher step-up and step-down voltage gains are required, more switches are needed. This control circuit becomes more complicated. In the three-level type, the voltage stress across the switches on the three-level type is only half of the conventional type. However, the step-up and step-down voltage gains are low. Since the sepic/zeta type is combined of two power stages, the conversion efficiency will be decreased. The switched capacitor and coupled-inductor types can provide high step-up and step-down voltage gains. However, their circuit configurations are complicated. Fig. 1 shows the conventional bidirectional DC-DC boost/buck converter, which is simple structure and easy control. However, the step-up and stepdown voltage gains are low.

A modified DC-DC boost converter is presented . The voltage gain of this converter is higher than the conventional DC-DC boost converter. Based on this converter, a novel bidirectional DC-DC converter is proposed, as shown in Fig. 2. The proposed converter employs a coupled inductor with same winding turns in the primary and secondary sides. Comparing to the proposed converter and the conventional bidirectional boost/buck converter, the proposed converter has the following advantages: 1) higher step-up and step-down voltage gains; 2) lower average value of the switch-current under same electric specifications. The following sections will describe the operating principles and steady-state analysis for the step-up and step-down modes. In order to analyze the steady-state characteristics of the proposed converter, some conditions are assumed as: 1) The ON-state resistance $R_{DS(ON)}$ of the switches and the equivalent series resistances of the coupled inductor and capacitors are ignored. 2) The capacitor is sufficiently large, and the voltages across the capacitor can be treated as constant.

II. STEP-UP MODE

The proposed converter in step-up mode is shown in Fig. 3. The pulse-width modulation (PWM) technique is used to control the switches S_1 and S_2 simultaneously. The switch S_3 is the synchronous rectifier.

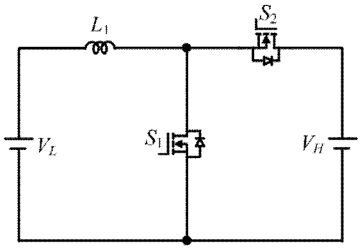

Fig. 1. Conventional bidirectional DC-DC boost/buck converter.

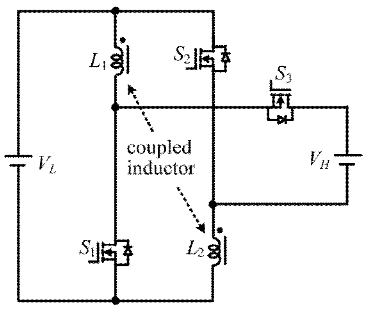

Fig. 2. Proposed bidirectional DC-DC converter.

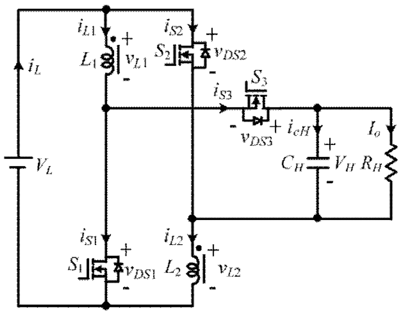

Fig. 3. Proposed converter in step-up mode.

Since the primary and secondary winding turns of the coupled inductor is same, the inductance of the coupled inductor in the primary and secondary sides are expressed as

$$L_1 = L_2 = L \quad (1)$$

Thus, the mutual inductance M of the coupled inductor is given by

$$M = k\sqrt{L_1 L_2} = kL \quad (2)$$

where k is the coupling coefficient of the coupled inductor. The voltages across the primary and secondary windings of the coupled inductor are as follows:

$$v_{L1} = L_1\frac{di_{L1}}{dt} + M\frac{di_{L2}}{dt} = L\frac{di_{L1}}{dt} + kL\frac{di_{L2}}{dt} \quad (3)$$

$$v_{L2} = M\frac{di_{L1}}{dt} + L_2\frac{di_{L2}}{dt} = kL\frac{di_{L1}}{dt} + L\frac{di_{L2}}{dt} \quad (4)$$

Fig. 4 shows some typical waveforms in continuous conduction mode (CCM) and discontinuous conduction mode (DCM). The operating principles and steady-state analysis of CCM and DCM are described as follows:

CCM Operation

Mode 1: During this time interval $[t_0, t_1]$, S_1 and S_2 are turned on and S_3 is turned off. The current flow path is shown in Fig. 5(a). The energy of the low-voltage side V_L is transferred to the coupled inductor. Meanwhile, the primary and secondary windings of the coupled inductor are in parallel. The energy stored in the capacitor C_H is discharged to the load. Thus, the voltages across L_1 and L_2 are obtained as

$$v_{L1} = v_{L2} = V_L \quad (5)$$

Substituting (3) and (4) into (5), yielding

$$\frac{di_{L1}(t)}{dt} = \frac{di_{L2}(t)}{dt} = \frac{V_L}{(1+k)L}, \quad t_0 \le t \le t_1 \quad (6)$$

Mode 2: During this time interval $[t_1, t_2]$, S_1 and S_2 are turned off and S_3 is turned on. The current flow path is shown in Fig. 5(b). The low-voltage side V_L and the coupled inductor are in series to transfer their energies to the capacitor C_H and the load. Meanwhile, the primary and secondary windings of the coupled inductor are in series. Thus, the following equations are found to be

$$i_{L1} = i_{L2} \quad (7)$$

$$v_{L1} + v_{L2} = V_L - V_H \quad (8)$$

Substituting (3), (4), and (7) into (8), yielding

$$\frac{di_{L1}(t)}{dt} = \frac{di_{L2}(t)}{dt} = \frac{V_L - V_H}{2(1+k)L}, \quad t_1 \le t \le t_2 \quad (9)$$

By using the state-space averaging method, the following equation is derived from (6) and (9):

$$\frac{DV_L}{(1+k)L} + \frac{(1-D)(V_L - V_H)}{2(1+k)L} = 0 \quad (10)$$

Simplifying (10), the voltage gain is given as

$$G_{CCM\,step\,up} = \frac{V_H}{V_L} = \frac{1+D}{1-D} \quad (11)$$

$V_L \qquad 1-D$

B. DCM Operation

Mode 1: During this time interval $[t_0, t_1]$, S_1 and S_2 are turned on and S_3 is turned off. The current flow path is shown in Fig. 5(a). The operating principle is same as that for the mode 1 of CCM operation. From (6), the two peak currents through the primary and secondary windings of the coupled inductor are given by

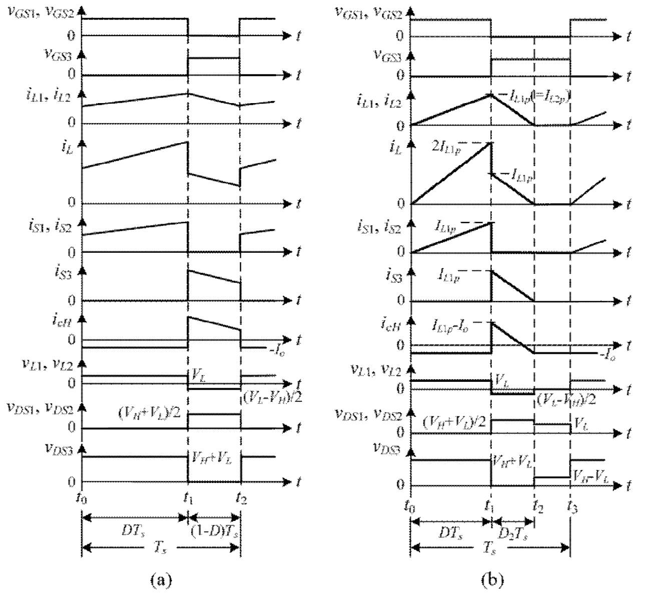

Fig. 4. Some typical waveforms of the proposed converter in step-up mode. (a) CCM operation. (b) DCM operation.

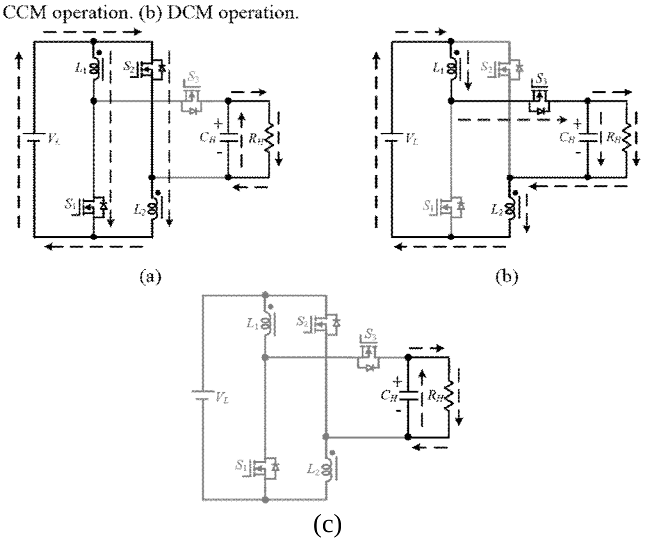

Fig. 5. Current flow path of the proposed converter in step-up mode. (a) Mode 1. (b) Mode 2. (c) Mode 3 for DCM operation.

$$I_{Lp1} = I_{Lp2} = \frac{V_L D T_s}{(1+k)L} \qquad (12)$$

2) Mode 2: During this time interval $[t_1, t_2]$, S_1 and S_2 are turned off and S_3 is turned on. The current flow path is shown in Fig. 5(b). The low-voltage side V_L and the coupled inductor are in series to transfer their energies to the capacitor C_H and the load. Meanwhile, the primary and secondary windings of the coupled inductor are in series. The currents, i_{L1} and i_{L2}, through the primary and secondary windings of the coupled inductor are decreased to zero at $t = t_2$. From (9), another expression of I_{L1p} and I_{L2p} is given by

$$I_{1p} = I_{2p} = \frac{(V_H - V_L) D_2 T_s}{2(1+k)L} \qquad (13)$$

3) Mode 3: During this time interval $[t_2, t_3]$, S_1 and S_2 are still turned off and S_3 is still turned on. The current flow path is shown in Fig. 5(c). The energy stored in the coupled inductor is zero. Thus, i_{L1} and i_{L2} are equal to zero. The energy stored in the capacitor C_H is discharged to the load.

From (12) and (13), D_2 is derived as follows:

$$D_2 = \frac{2DV_L}{V_H - V_L} \qquad (14)$$

From Fig. 4(b), the average value of the output-capacitor current during each switching period is given by

$$I_{cH} = \frac{\frac{1}{2} D_2 T_s I_{Lp1} - I_o T_s}{T_s} = \frac{D_2 I_{Lp1}}{2} - I_o \qquad (15)$$

Substituting (12) and (14) into (15), I_{cH} is derived as

$$I_{cH} = \frac{D^2 V_L^2 T_s}{(1+k)L(V_H - V_L)} - \frac{V_H}{R_H} \qquad (16)$$

Since I_{cH} is equal to zero under steady state, equation (16) can be re-written as follows:

$$\frac{D^2 V_L^2 T_s}{(1+k)L(V_H - V_L)} = \frac{V_H}{R_H} \qquad (17)$$

Then, the normalized inductor time constant is defined as

$$\tau_{LH} = \frac{L}{R_H T_s} = \frac{L f_s}{R_H} \qquad (18)$$

where f_s is the switching frequency.

Substituting (18) into (17), the voltage gain is given by

$$G_{DCM\,step\,up} \equiv \frac{V_H}{V_L} = \frac{1}{2} + \sqrt{\frac{1}{4} + \frac{D^2}{(1+k)\tau_{LH}}} \quad (19)$$

C. Boundary Operating Condition of CCM and DCM

When the proposed converter in step-up mode is operated in boundary conduction mode (BCM), the voltage gain of CCM operation is equal to the voltage gain of DCM operation. From (11) and (19), the boundary normalized inductor time constant $\tau_{LH,B}$ can be derived as follows:

$$\tau_{LH,B} = \frac{D(1-D)^2}{2(1+k)(1+D)} \quad (20)$$

The curve of $\tau_{LH,B}$ is plotted in Fig. 6. If τ_{LH} is larger than $\tau_{LH,B}$, the proposed converter in step-up mode is operated in CCM.

(assuming k =1).

Fig. 7 shows the proposed converter in step-down mode. The PWM technique is used to control the switch S_3. The switches S_1 and S_2 are the synchronous rectifiers. Fig. 8 shows some typical waveforms in CCM and DCM. The operating principle and steady-state analysis of CCM and DCM are described as follows:

A. CCM Operation

Mode 1: During this time interval [t_0, t_1], S_3 is turned on and S_1/S_2 are turned off. The current flow path is shown in Fig. 9(a). The energy of the high-voltage side V_H is transferred to the coupled inductor, the capacitor C_L, and the load. Meanwhile, the primary and secondary windings of the coupled inductor are in series. Thus, the following equations are given as

$$i_{L1} = i_{L2} \quad (21)$$

$$v_{L1} + v_{L2} = V_H - V_L \quad (22)$$

Substituting (3), (4), and (21) into (22), yielding

$$\frac{di_{L1}(t)}{dt} = \frac{di_{L2}(t)}{dt} = \frac{V_H - V_L}{2(1+k)L}, \quad t_0 \le t \le t_1 \quad (23)$$

Mode 2: During this time interval [t_1, t_2], S_3 is turned off and S_1/S_2 are turned on. The current flow path is shown in Fig. 9(b). The energy stored in the coupled inductor is released to the capacitor C_L and the load. Meanwhile, the primary and secondary windings of the coupled inductor are in parallel. Thus, the voltages across L_1 and L_2 are derived as

$$v_{L1} = v_{L2} = -V_L \quad (24)$$

Substituting (3) and (4) into (24), yielding

$$\frac{di_{L1}(t)}{dt} = \frac{di_{L2}(t)}{dt} = \frac{-V_L}{(1+k)L}, \quad t_1 \le t \le t_2 \quad (25)$$

By using the state-space averaging method, the following equation is obtained from (23) and (25):

t t t t t
t
t
t
t t

(c)

Fig. 9. Current flow path of the proposed converter in step-down mode. (a) Mode 1. (b) Mode 2. (c) Mode 3 for DCM operation.

Simplifying (26), the voltage gain is found to be

$$G_{CCM\,step\,down} \equiv \frac{V_L}{V_H} = \frac{D}{2-D} \quad (27)$$

B. DCM Operation

The operating modes can be divided into three modes, defined as modes 1, 2, and 3.

Mode 1: During this time interval [t_0, t_1], S_3 is turned on and S_1/S_2 are turned off. The current flow path is shown in Fig. 9(a). The operating principle is same as that for the mode 1 of CCM operation. From (23), the two peak currents through the primary and secondary windings of the coupled inductor are given by

$$I_{Lp1} = I_{Lp2} = \frac{(V_H - V_L)DT_s}{2(1+k)L} \quad (28)$$

Mode 2: During this time interval [t_1, t_2], S_3 is turned off and S_1/S_2 are turned on. The current flow path is shown in Fig. 9(b). The energy stored in the coupled inductor is released to the capacitor C_L and the load. Meanwhile, the primary and secondary windings of the coupled inductor are in parallel.

The currents, i_{L1} and i_{L2}, through the primary and secondary windings of the coupled inductor are decreased to zero at $t = t_2$.

From (25), another expression of I_{L1p} and I_{L2p} is given as

V D T^L 2 ——— *s*

(29)

$^{I}1_p$ □ □$^{I}2_p$

(1□*k L*)

Mode 3: During this time interval [t_2, t_3], S_3 is still turned off and S_1/S_2 are still turned on. The current flow path is shown in Fig. 9(c). The energy stored in the coupled inductor is zero. Thus, i_{L1} and i_{L2} are equal to zero. The energy stored in the capacitor C_L is discharged to the load.

From (28) and (29), D_2 is derived as follows:

D(*V^H* □*V^L*) ——— (30)

$^{D}2$ □

2*VL*

From Fig. 9(b), the average value of the output-capacitor current during each switching period is given by

1 1

*DT Is L p*1 □ *D T*2 *s* (2*IL p*1)□*I To s*

IcL □ 2 2 ———

T_s

□ $\frac{1}{2}$ $D I_{Lp1}$ □ $^{D}I_{21Lp}$ □ $^{I}{}_o$ (31)

Substituting (28) and (30) into (31), I_{cL} is derived as

*D T*2 *s* □ 4(1□*k LV*) *L* R_L

IcL □ □(*VH* □*V VL*) *L* □(*VH* □*VL*)2 □□□ *VL*

(32)

Since I_{cL} is equal to zero under steady state, equation (32) can be re-written as follows:

D T^{2s} □□(*V^H* □*V V^L*) *L* □(*V^H* □*V^L*)^2 □□ □ *VL* (33)

4(1□*k LV*) *L* R_L

Then, the normalized inductor time constant is defined as

L *Lf^s* —— (34)

□*LL* □ □

RL sT *RL*

Substituting (34) into (33), the voltage gain of DCM operation is given by

VL ——2 (35)

GDCM step down(□) □ □ V_H 1□ 1□16(1□k_2)□$_{LL}$

D

C. Boundary Operating Condition of CCM and DCM

When the proposed converter in step-down mode is operated in BCM, the voltage gain of CCM operation is equal to the voltage gain of DCM operation. From (27) and (35), the boundary normalized inductor time constant $\tau_{LL,B}$ can be derived as follows:

(1□*D*)(2□*D*)

□$_{LL B,}$ □ ———— (36) 2(1□*k*)

The curve of $\tau_{LL,B}$ is plotted in Fig. 10. If τ_{LL} is larger than $\tau_{LL,B}$, the proposed converter in the step-down mode is operated

in CCM.

IV. COMPARISON OF THE PROPOSED CONVERTER AND CONVENTIONAL BIDIRECTIONAL BOOST/BUCK CONVERTER

A. Voltage Gain

The curves of the voltage gain of the proposed converter and conventional bidirectional boost/buck converter in CCM operation are plotted in Fig. 11. It is seen that the step-up and step-down voltage gains of the proposed converter are higher than the conventional bidirectional boost/buck converter.

B. Voltage Stress on the Switches

From Figs. 4(a) and 8(a), the voltage stresses on S_1, S_2, and S_3 in the proposed converter are derived as

□ *VH* □*VL*

□ □*VDS*1 □*VDS*2 □ 2 (37)

□□*VDS*3 □*VH* □*VL*

As to the voltage stresses on S_1 and S_2 in the conventional bidirectional boost/buck converter are given as

V_{DS1} □$^{V}{}_{DS2}$ □$^{V}{}_{H}$ (38)

Therefore, if the proposed converter is used for high stepup/down voltage-gain application, the rated voltage of S_1 and S_2 in the proposed converter can be selected to be lower than the conventional converter. Also, the rated voltage of S_3 in the

(assuming k =1). (b)

(b) Fig. 11. Voltage gain of the proposed converter and conventional bidirectional boost/buck converter in CCM operation. (a) Step-up mode. (b) Step-down mode.
proposed converter can be selected as same as the conventional converter.

C. Average Value of the Switch-Current

When the proposed converter in step-up mode is operated in CCM, the average value of the input current i_L is found from Fig. 4(a).

2IL1(proposed)DTs □*IL1(proposed)* (1□*D T*) *s*
IL proposed( ) □

T_s
□ □(1 *D I*) $_{L1(proposed)}$ (39)

where I_{L1} is the average value of i_{L1}. When the conventional bidirectional boost/buck converter in step-up mode is also operated in CCM, the average value of the input current i_L is given by

IL conventional( ) □ *IL conventional1*( ) (40)

Under same electric specifications for the proposed converter and conventional bidirectional boost/buck converter, the input power can be expressed as

Pin □*V IL L conventional*() □*V IL L proposed*( )
(41)
Substituting (39) and (40) into (41), yielding
IL conventional1()
$I_{L1(proposed)}$ □ (42)
1□*D*

When the proposed converter in step-down mode is operated in CCM, the average value of the current i_{LL} is found from Fig. 8(a).

IL1(proposed)DTs □*2IL1(proposed)*(1□ *D T*) *s*
ILL proposed( ) □

T_s
□ (2□ *D I*) $_{L1(proposed)}$ (43)

Under same electric specifications for the proposed converter and conventional bidirectional boost/buck converter, the output power can be obtained as

Po □*V IL L conventional1*( ) □*V IL LL proposed*( ) (44)

From (43) and (44), the following equation is derived as
IL conventional1()
$I_{L1(proposed)}$ □ (45)
2□*D*

From (42) and (45), one can know that the average value of the switch-current in the proposed converter is less than the conventional bidirectional boost/buck converter.

D. Efficiency Analysis

For the proposed converter, the equivalent circuits in stepup mode are shown in Fig. 12. r_{L1} and r_{L2} represent the equivalent series resistor (ESR) of the primary and secondary windings of the coupled inductor. r_{S1}, r_{S2}, and r_{S3} denote the ON-state resistance of S_1, S_2, and S_3. When S_1/S_2 are turned on and S_3 is turned off, the equivalent circuit is shown in Fig. 12(a). The average values of i_{cH} and v_{L1} are obtained as

I VH (46)

I_{cH} □ □ *RH*
V_{L1}^{I} □ □$V_L I_{L1}(r_{L1}$ □$r_{S1})$ (47)

When S_1/S_2 are turned off and S_3 is turned on, the equivalent circuit is shown in Fig. 12(b). The average values of i_{cH} and v_{L1} are derived as

I_{cHII} □ □I_{L1} *VH*
(48)

RH
II *VL* □*VH* □*IL1*(*rL1* □ □*rS3* *rL2*)
(49)

V_{L1} □
2

(b)

Fig. 12. Equivalent circuit of the proposed converter in step-up mode. (a) S_1/S_2 ON and S_3 OFF. (b) S_1/S_2 OFF and S_3 ON.
By using the ampere-second balance principle on C_H, the following equations are obtained as

DT_s $(1-D)T_s$
$\int I\, dt\, c_H^I + \int I\, dt\, c_H^{II} = 0$ (50)

0

Substituting (46) and (48) into (50), I_{L1} is given by

$$I_{L1} = \frac{V_H}{(1-D)R_H} \quad (51)$$

Using the volt-second balance principle on L_1 yields

DT_s $(1-D)T_s$
$\int V\, dt_{L1}^I + \int V\, dt_{L1}^{II} = 0$ (52)

0

Substituting (47) and (49) into (52), the actual voltage gain is derived as

V_H □1□ D □ 2 (1□ D R)^2 H (53)
V_L 1□D (1□ D R) H □2 (D r_{L1} □r_{S1}) (1□ □D r)($L1$ □r_{S3} □r_{L2})

The input power and output power are obtained as

(1□ D)V VL H (54)

Pin □ 2V I D V IL $L1$ □ L $L1$(1□ D) □
(1□D)R_H

$$P_o = \frac{V_H^2}{R_H} \quad (55)$$

From (53)-(55), the efficiency is found to be

□□ □Po 2
(1□D R)2H (56)

P_{in} (1□D R)$_H$ □2 (D r_{L1} □ □ □r_{S1}) (1 D r)($L1$ □ □r_{S3} r_{L2})

For the proposed converter, the equivalent circuits in stepdown mode are shown in Fig. 13. When S_3 is turned on and S_1/S_2 are turned off, the equivalent circuit is shown in Fig. 13(a). The average values of i_{cL} and v_{L1} are obtained as

$$I_{cL}^I = I_{L1} - \frac{V_L}{R_L} \quad (57)$$

V_{L1}^I □ V_H □ □V_L I_{L1}(r_{S3} □ □r_{L1} r_{L2}) (58)

2

When S_3 is turned off and S_1/S_2 are turned on, the equivalent circuit is shown in Fig. 13(b). The average values of i_{cL} and v_{L1} are derived as

S_1/S_2 ON and S_3 OFF. (b) S_1/S_2 OFF and S_3 ON.

I_{cL}^{II} □2I_{L1} □$\frac{V_L}{R_L}$ (59)

V_{L1}^{II} □□ □V_L I_{L1}(r_{L1} □r_{S1}) (60)

By using the ampere-second balance principle on C_L, the following equations are obtained as

DT_s $(1-D)T_s$
$\int I\, dt_{cL}^I + \int I\, dt_{cL}^{II} = 0$ (61)

0

Substituting (57) and (59) into (61), I_{L1} is obtained as

$$I_{L1} = \frac{V_L}{(2-D)R_L} \quad (62)$$

Using the volt-second balance principle on L_1 yields

DT_s $(1-D)T_s$
$\int V\, dtL_1^I + \int V\, dtL_1^{II} = 0$ (63)

0

Substituting (58) and (60) into (63), the actual voltage gain is derived as

V_L □ D □ 2 (2□D R)^2 L (64)
V_H 2□D (2□D R) L □ D r($S3$ □r_{L1} □r_{L2}) 2(1□ □D r)($L1$ □r_{S1})

The input power and output power are obtained as

DV VL (65)

Pin □V I DH $L1$ □
(2□D)R_L

$$P_o = \frac{V_L^2}{R_L} \quad (66)$$

From (64)-(66), the efficiency is found to be

2

Po $(2 D R)L$ (67)

P_{in} $(2 D R)$ $_L$ D $r($ $_{S3}$ r_{L1} $r_{L2})$

$2(1$ $D r)($ $_{L1}$ $r_{S1})$

For the conventional converter, the equivalent circuits in step-up mode are shown in Fig. 14. r_{L1} represents the ESR of the inductor. r_{S1} and r_{S2} denote ON-state resistance of S_1 and S_2. According to the foregoing method, the efficiency is derived as follows:

P_o $(1 D R)2$ $_H$ (68)

P_{in} $(1 D R)$ $_H$ D $r($ $_{L1}$ $r_{S1})$ $(1$ $D r)($ $_{L1}$ $r_{S2})$

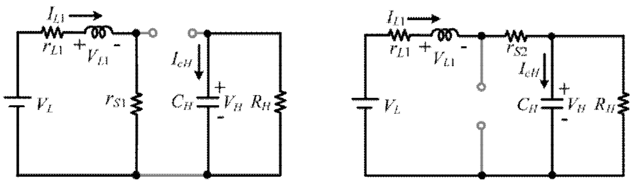

(b)

Fig. 14. Equivalent circuit of the conventional converter in step-up mode. (a) S_1 ON and S_2 OFF. (b) S_1 OFF and S_2 ON.

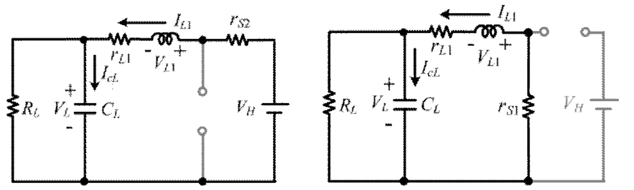

(b)

Fig. 15. Equivalent circuit of the conventional converter in step-down mode.

S_2 ON and S_1 OFF. (b) S_2 OFF and S_1 ON.

For the conventional converter, the equivalent circuits in step-down mode are shown in Fig. 15. According to the foregoing method, the efficiency is derived as follows:

Po

RL (69)

Pin RL $D r(S2$ $rL1) (1 D r)(L1$ $rS1)$

In order to compare the calculated efficiency for the proposed converter and the conventional converter, some parameters of three cases are assumed as follows:

Case 1: $r_{L1} = r_{L2} = 11$ mΩ, $r_{S1} = r_{S2} = r_{S3} = 23$ mΩ, $V_H = 42$ V, and $V_L = 21$ V.

Case 2: $r_{L1} = r_{L2} = 11$ mΩ, $r_{S1} = r_{S2} = r_{S3} = 23$ mΩ, $V_H = 42$ V, and $V_L = 14$ V.

Case 3: $r_{L1} = r_{L2} = 11$ mΩ, $r_{S1} = r_{S2} = r_{S3} = 23$ mΩ, $V_H = 42$ V, and $V_L = 10.5$ V.

Substituting these parameters into (56) and (67)-(69), the calculated efficiencies of the proposed and conventional converters in step-up and step-down modes are shown in Figs. 16 and 17, respectively. Thus, if the lower voltage gain is required, the conventional converter can be selected for lower cost. If the higher voltage gain is required, the proposed converter can be chosen for higher efficiency.

V. EXPERIMENTAL RESULTS

In order to verify the performance of the proposed converter, a 14/42-V prototype circuit is built in the laboratory for the automobile dual-battery system. The electric specifications and circuit components are selected as $V_L = 14$ V, $V_H = 42$ V, $f_s = 50$ kHz, $P_o = 200$ W, $C_L = C_H = 330$ μF, $L_1 = L_2 = 15.5$ μH ($r_{L1} = r_{L2} = 11$ mΩ). Also, MOSFET IRF3710 ($V_{DSS} = 100$ V, $R_{DS(ON)} = 23$ mΩ, and $I_D = 57$ A) is selected for S_1, S_2, and S_3.

Some experimental results in step-up and step-down modes are shown in Figs. 18 – 21. Fig. 18(a) shows the waveforms of the input current i_L and the coupled-inductor currents, i_{L1} and i_{L2}, in step-up mode. It can be seen that i_{L1} is equal to i_{L2}. The current i_L is double of the level of the coupled-inductor current during S_1/S_2 ON-period and equals the coupled-inductor

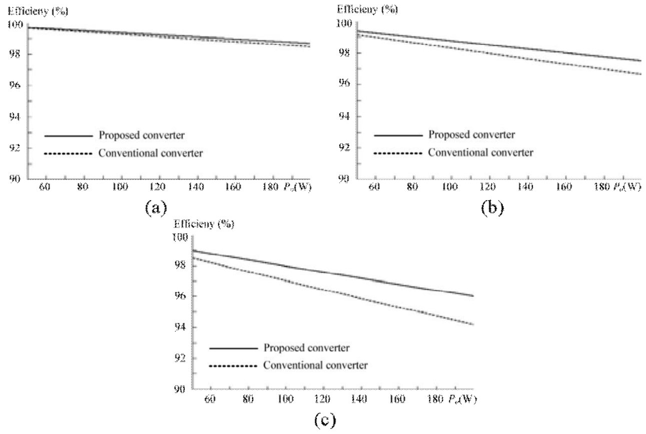

Fig. 16. Calculated efficiency of the proposed and conventional converters in step-up mode. (a) Case 1. (b) Case 2. (c) Case 3.

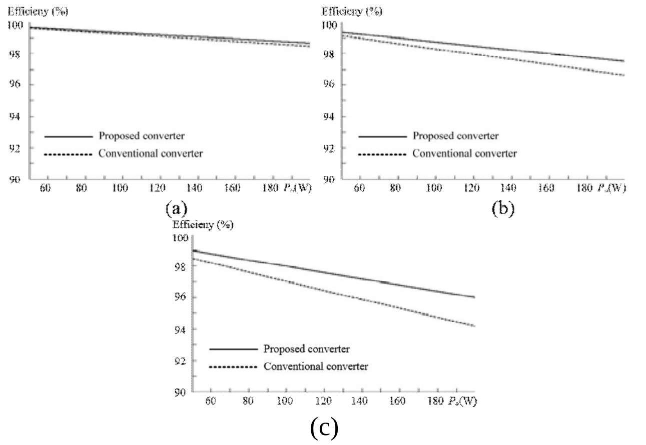

Fig. 17. Calculated efficiency of the proposed and conventional converters in step-down mode. (a) Case 1. (b) Case 2. (c) Case 3.

current during S_1/S_2 OFF-period. Fig. 20(a) shows the waveforms of the current i_{LL} and the coupled-inductor currents, i_{L1} and i_{L2}, in step-down mode. It can be observed that i_{L1} is equal to i_{L2}. The current i_{LL} equals to the coupled-inductor current during S_3 ON-period and is double of the level of the coupled-inductor current during S_3 OFF-period. Figs. 18(b) and 20(b) show the waveforms of the switch-current, i_{S1}, i_{S2}, and i_{S3}, in step-up and step-down modes, respectively. As can be seen in Figs. 18(c) and 20(c), the voltage stresses on S_1 and S_2 equal $(V_H+V_L)/2$. Also, the voltage stress on S_3 equals V_H+V_L. Figs. 19 and 21 show the dynamic response of the proposed converter in step-up and step-down modes. One can see that the output voltage is well regulated.

Moreover, the prototype circuit of the conventional bidirectional boost/buck converter is also implemented in the laboratory. The electric specifications and circuit components are selected as V_L = 14 V, V_H = 42 V, f_s = 50 kHz, P_o = 200 W, L_1 = 28 μH (r_{L1} = 15 mΩ), C_L = C_H = 330 μF. Also, MOSFET IRF3710 is selected for S_1 and S_2. The measured efficiency in the proposed converter and the conventional bidirectional boost/buck converter are shown in Fig. 22. At full-load condition, the measured efficiency of the proposed converter is 92.7% in step-up mode and is 93.7% in step-down mode. Also, the measured efficiency of the proposed converter is around 92.7%-96.2% in step-up mode and is around 93.7%-96.7%. Also, it is seen from Fig. 22 that the measured efficiency of the proposed converter are higher than the conventional bidirectional boost/buck converter.

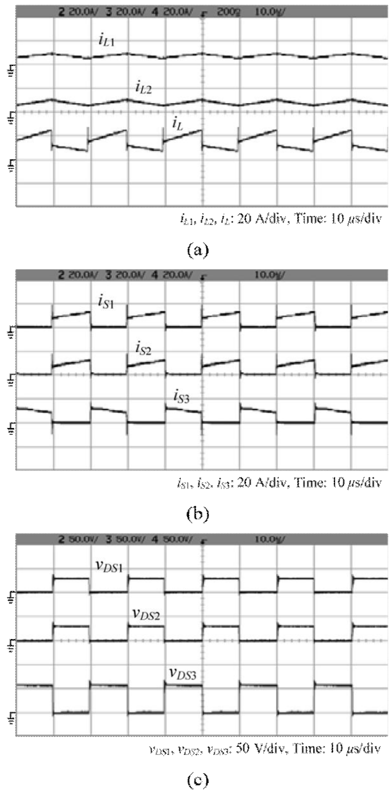

Fig. 18. Some experimental waveforms of the proposed converter in step-up mode. (a) i_{L1}, i_{L2}, and i_L, (b) i_{S1}, i_{S2} ,and i_{S3}. (c) v_{DS1}, v_{DS2}, and v_{DS3}.

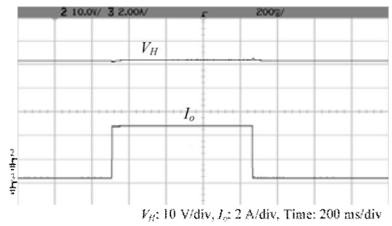

Fig. 19. Dynamic response of the proposed converter in step-up mode for the output power variation between 20 W and 200 W.

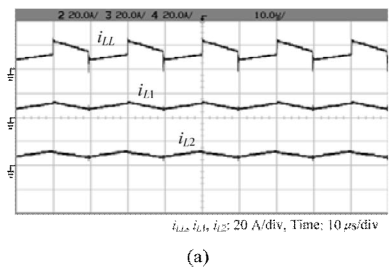

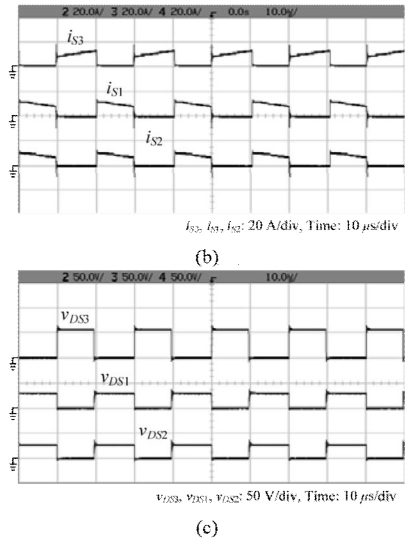

Fig. 20. Some experimental waveforms of the proposed converter in step-down mode. (a) i_{LL}, i_{L1}, and i_{L2}, (b) i_{S3}, i_{S1}, and i_{S2}. (c) v_{DS3}, v_{DS1}, and v_{DS2}.

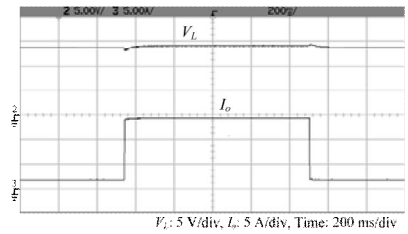

Fig. 21. Dynamic response of the proposed converter in step-down mode for the output power variation between 20 W and 200 W.

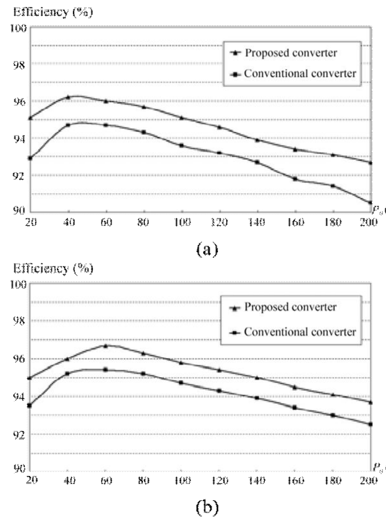

Fig. 22. Measured efficiency in the proposed converter and conventional bidirectional boost/buck converter. (a) Step-up mode. (b) Step-down mode.

VI. CONCLUSIONS

This paper researches a novel bidirectional DC-DC converter. The circuit configuration of the proposed converter is very simple. The proposed converter has higher step-up and stepdown voltage gains and lower average value of the switchcurrent than the conventional bidirectional boost/buck converter. From the experimental results, it is see that the experimental waveforms agree with the operating principle and steady-state analysis. At full-load condition, the measured efficiency is 92.7% in step-up mode and is 93.7% in step-down mode. Also, the measured efficiency is around 92.7%-96.2% in step-up mode and is around 93.7%-96.7%, which are higher than the conventional bidirectional boost/buck converter.

REFERENCES

[1] J. A. Rosero, J. A. Ortega, E. Aldabas, and L. Romeral, "Moving towards a more electric aircraft," IEEE Aerosp. Electron. Syst. Mag., vol. 22, no. 3, pp. 3–9, Mar. 2007.

[2] A. Hamadi, S. Rahmani, and K. Al-Haddad, "A hybrid passive filter configuration for VAR control and harmonic compensation," IEEE Trans. Ind. Electron., vol. 57, no. 7, pp. 2419–2434, Jul. 2010.

[3] A. Varschavsky, J. Dixon, M. Rotella, and L. Moran, "Cascaded nine-level inverter for hybrid-series active power filter, using industrial controller," IEEE Trans. Ind. Electron., vol. 57, no. 8, pp. 2761–2767, Aug. 2010.

[4] A. Luo, X. Xu, L. Fang, H. Fang, J. Wu, and C. Wu, "Feedback– feedforward PI-type iterative learning control strategy for hybrid active power filter with injection circuit," IEEE Trans. Ind. Electron., vol. 57, no. 11, pp. 3767–3779, Nov. 2010.

[5] S. Rahmani, N. Mendalek, and K. Al-Haddad, "Experimental design of a nonlinear control technique for three-phase shunt active power filter," IEEE Trans. Ind. Electron., vol. 57, no. 10, pp. 3364–3375, Oct. 2010.

[6] B. Singh and J. Solanki, "An implementation of an adaptive control al-gorithm for a three-phase shunt active filter," IEEE Trans. Ind. Electron., vol. 56, no. 8, pp. 2811–2820, Aug. 2009.

[7] A. Bhattacharya and C. Chakraborty, "A shunt active power filter with enhanced performance using ANN-based predictive and adaptive con-trollers," IEEE Trans. Ind. Electron., vol. 58, no. 2, pp. 421–428, Feb. 2011.

[8] D. Ganthony and C. M. Bingham, "Integrated series active filter for aerospace flight control surface actuation," in Proc. EPE, 2007, pp. 1–9.

[9] E. Lavopa, E. Summer, P. Zanchetta, C. Ladisa, and F. Cupertimo, "Real-time estimation of fundamental frequency and harmonics for active power filters applications in aircraft electrical systems," in Proc. EPE, 2007, pp. 4220–4229.

[10] E. Lavopa, M. Summer, P. Zanchetta, C. Ladisa, and F. Cupertimo, "Real-time estimation of fundamental frequency and harmonics for active power filters applications in aircraft electrical systems," IEEE Trans. Ind. Electron., vol. 56, no. 8, pp. 2875–2884, Aug. 2009.

[11] M. Odavic, P. Zanchetta, and M. Summer, "A low switching frequency high bandwidth current control for active shunt power filter in aircrafts power networks," in Proc. IEEE IECON, 2007, pp. 1863–1868.

[12] V. Biagini, M. Odavic, P. Zanchetta, M. Degano, and P. Bolognesi, "Im-proved dead beat control of a shunt active filter for aircraft power sys-tems," in Proc. IEEE ISIE, 2010, pp. 2702–2707.

[13] H. Hu, W. Shi, J. Xue, Y. Lu, and Y. Xing, "A multiresolution control strategy for DSP controlled 400 Hz shunt active power filter in an aircraft power system," in Proc. IEEE APEC, 2010, pp. 1785–1791.

[14] A. Eid, M. Abdel-Salam, H. El-Kishky, and T. El-Mohandes, "Active power filters for harmonic cancellation in conventional and advanced aircraft electric power systems," Elect. Power Syst. Res., vol. 79, no. 1, pp. 80–88, Jan. 2009.